



Analytical models of flow availability in two-layer networks with dedicated path protection

Wenda Ni ^{a,*}, Jing Wu ^b, Changcheng Huang ^a, Michel Savoie ^b

^a Department of Systems and Computer Engineering, Carleton University, Ottawa, Ontario, Canada K1S 5B6

^b Communications Research Centre Canada, Ottawa, Ontario, Canada K2H 8S2

ARTICLE INFO

Available online 4 August 2012

Keywords:

Two-layer networks
Flow availability analysis
Dedicated path protection

ABSTRACT

Even with protection, user traffic flows can be disrupted due to network failures that are beyond the protection capability. One of the quantitative metrics to measure the service quality in such a context is “availability”. We study analytical models that compute availability of upper-layer flows in two-layer networks with dedicated path protection at either the upper or the lower layer. Our investigations reveal that existing analytical models significantly overestimate availability requirements on lower-layer links, and exaggerate upper-layer flow unavailability by treating correlated upper-layer failures as being independent. In contrast, our proposed model takes into account such correlations by tracing upper-layer failures to lower-layer root causes, thus greatly relaxing unnecessary high-availability requirements on lower-layer links without compromising the availability of upper-layer flows. In our simulation examples, using the existing models, up to 66.6% and 89.2% of the total flows are overestimated on their unavailability under dedicated path protection at the upper and the lower layer, respectively. Moreover, the average unavailability redundancy built into these flows is about 30% and 15% for protection at the upper and the lower layer, respectively. Furthermore, we compare flow availability under the two protection schemes, and show that given the same initial unprotected network states, protection at the lower layer enjoys lower average flow unavailability than protection at the upper layer.

© 2012 Elsevier B.V. All rights reserved.

1. Introduction

Aiming at improving network failure resilience and providing reliable communication services, network protection is used as a proactive recovery procedure, where spare capacity is reserved during the request setup to tolerate a limited set of network failures, e.g., against single fibre link failures in [1–3]. When a failure occurs within a pre-defined set, a flow is fully protected by a protection switchover mechanism, i.e., the flow maintains

100% service recovery. However, when a failure occurs outside of the pre-defined set, the flow becomes out of service. A quantitative assessment of how well a flow is protected in all network failures (both within and outside of the protection scope) is the “flow availability” metric, defined as a ratio of accumulated operating time of a flow over its lifespan.

In two-layer networks, service protection for upper-layer connections (i.e., flows) can be achieved by using path-based protection at the upper or the lower layer [1–3]. IP over optical networks adopt such a two-layer architecture, where a point-to-point link at the IP layer (i.e., the upper layer) is laid out as an end-to-end wavelength connection at the optical layer (i.e., the lower layer). In upper-layer protection, a flow is routed as a

* Corresponding author. Tel.: +1 613 790 6788.

E-mail addresses: wendani@sce.carleton.ca, wonda.ni@gmail.com (W. Ni), jing.wu@crc.gc.ca (J. Wu), huang@sce.carleton.ca (C. Huang), michel.savoie@crc.gc.ca (M. Savoie).

pair of upper-layer link-disjoint paths, which must also be lower-layer link-disjoint. An upper-layer link is realized as a single lower-layer path. In lower-layer protection, an upper-layer link is laid out as a pair of link-disjoint lower-layer paths, and a flow simply maintains a single upper-layer path. In this paper, we focus on using dedicated path protection against failures of lower-layer links, e.g., fibre links in IP over optical networks. As our discussions are immediately applicable to any layered structures characterized by a packet-switched network overlaid on top of a circuit-switched network, we will mainly use the terms “two-layer networks”, “upper layer”, and “lower layer” throughout the paper to be general. They are interchangeable with “IP over optical networks”, “logical/IP layer”, and “physical/optical layer”, respectively.

Flow availability is a key attribute in a service level agreement (SLA), a formal contract between a service provider and a customer [4]. Flow availability in an SLA specifies the maximum accumulated service outage time a customer could expect over the service duration. On one hand, higher flow availability generally requires more costly network resources. Thus, flow unavailability over-estimation means additional network costs in resource allocation and/or high-availability equipment for meeting a service guarantee. On the other hand, violations of flow availability in SLAs result in financial penalties to service providers, and have negative impacts on customer relationship. Therefore, a service provider relies on accurate estimation of flow availability to provide just enough flow availability, i.e., slightly above the flow availability requirement in an SLA, with minimum network resources to achieve maximum profit.

Different models were proposed to compute the availability of wavelength connections in optical networks, or generally, the availability of lower-layer connections in two-layer networks. These models employ either a series-parallel reliability block diagram method [5–7] or a network-wise Markov state-space method [8–10], which all assume that fibre links fail independently. Since a fibre link can carry multiple wavelength connections with the support of Wavelength Division Multiplexing (WDM) technology, one fibre link failure can lead to multiple correlated upper-layer link failures. It is observed in the Sprint backbone network that at least two logical links fail in an optical failure event, and the number of concurrently failed links can go up to 10 in the same event [11]. Due to the strong correlation in upper-layer link failures, a direct application of the abovementioned analytical models to upper-layer flows produces inaccurate results. Specifically, by treating correlated upper-layer link failures as independent, current flow availability model in [12–14] can significantly exaggerate flow unavailability, imposing unnecessary high-availability requirements on lower-layer links to satisfy a given flow availability value.

Apart from the previous works in [12–14], the work in [15] discussed minimum failure-probability routing on a special correlated link failure model, where in a shared risk link group (SRLG) failure, links associated with the SRLG fail independently with some probabilities (less than one). Also, SRLG events are assumed to be mutually exclusive in the sense that only one SRLG failure can occur

and exist in the network at a time. In the context of two-layer networks, the notion of SRLG, however, is deterministic. That is, in a lower-layer link failure, all lightpaths that traverse the lower-layer link fail. In addition, except the basic assumption on failure independence among lower-layer links, we do not make any specific limits on the number of lower-layer links that can fail concurrently in the network. The work in [16] studied the availability of logical topology in terms of connectivity while our focus is on the availability of upper-layer flows.

In this paper, we propose analytical models to compute flow availability in two-layer networks to address the challenges arising from the fundamental differences between link failures at the upper and the lower layers. The key principle in tackling failure correlation is to compute flow availability at the lower layer, where lower-layer link failures are mutually independent in our assumption. Our model only requires upper-layer topology layout information, i.e., the mapping of upper-layer links onto lower-layer paths. This mapping information is typically available to tier-1 carriers, such as AT&T [4,17] and Sprint [11], that own both layers of a backbone network. We consider dedicated path protection since it is the most widely deployed survivability scheme. Regarding where the protection is deployed, we consider two options: protection at the upper layer as today's carrier networks rely on the upper layer to provide survivability services [4,17], and protection at the lower layer, which is desirable for high-rate private line services [4]. The analytical results using our models match the simulation results much closer than the results using the existing model [12–14]. Our proposed models constitute the foundation for unavailability-minimized routing and unavailability-constrained routing. While we discuss flow availability models in the context of two-layer networks, the proposed approach is generally applicable to a class of correlated failure scenarios, where correlations among failures can be decomposed into a set of independent root causes through a certain mapping method. Our preliminary work on analytical model for protection at the upper layer was presented in [18].

The remainder of this paper is organized as follows: we present the network model with failure assumptions in Section 2. We propose flow availability models for protection at the upper and the lower layer in Sections 3 and 4, respectively, followed by numerical results in Section 5. We conclude this paper in Section 6.

2. Network model

The lower-layer topology is represented by an undirected graph $G_l = (\mathcal{N}_l, \mathcal{L}_l)$, where \mathcal{N}_l is the node set, and \mathcal{L}_l is the link set with links numbered from 1 to $|\mathcal{L}_l|$. Similarly, the upper-layer topology is modeled as $G_u = (\mathcal{N}_u, \mathcal{L}_u)$. We assume that each lower-layer node hosts no more than one upper-layer node from one upper-layer topology [19]. In other words, \mathcal{N}_u is a subset of \mathcal{N}_l , i.e., $\mathcal{N}_u \subseteq \mathcal{N}_l$. Let \mathcal{D}_u denote a given set of user traffic flows that need to be serviced, i.e., the upper-layer flow set.

We characterize lower-layer link failures and repairs with the following typical assumptions:

- Each lower-layer link has two states; that is, an up (operating) state and a down (failed) state.
- All lower-layer links fail independently.
- Time to failure and failure repair time of lower-layer link i follow negative exponential distributions with the mean failure rate and the mean repair rate denoted by λ_i and ω_i , respectively.
- Each lower-layer link i has a steady-state availability value A_i . The steady-state availability, or simply availability, represents the long-term probability that link i is in the up state. The value of A_i is given by

$$A_i = \frac{\omega_i}{\omega_i + \lambda_i} = \frac{MTTF_i}{MTTF_i + MTTR_i}, \quad i \in \mathcal{L}_l, \quad (1)$$

where $MTTF_i = 1/\lambda_i$ and $MTTR_i = 1/\omega_i$ are the mean time to failure (MTTF) and the mean time to repair (MTTR) of link i , respectively.

- Let U_i denote the unavailability of lower-layer link i . We have

$$U_i \equiv 1 - A_i \ll 1, \quad i \in \mathcal{L}_l. \quad (2)$$

- In a lower-layer link failure, all lower-layer paths traversing the link fail simultaneously.
- Protection is provided at either the upper layer or the lower layer, but not both.
- A protection switchover does not cause any service disruption.

3. Flow availability model for protection at the upper layer

3.1. Survivable mapping for dedicated path protection at the upper layer

When protection is deployed at the upper-layer, each upper-layer link j is laid out as one single lower-layer path θ_j . The upper-layer topology layout is described by the interlayer link mapping matrix $\Theta = \{\theta_j\}_{|\mathcal{L}_u| \times 1} = \{\theta_{ji}\}_{|\mathcal{L}_u| \times |\mathcal{L}_l|}$, where binary element θ_{ji} equals one if upper-layer link j uses lower-layer link i ; equals zero otherwise.

To protect against single lower-layer link failures, survivability requirement must be satisfied for mapping upper-layer links to lower-layer paths: *once the mapping is made, for each upper-layer node pair, there exist at least two paths that are link-disjoint at both the upper and the lower layers*. Obtaining such a survivable mapping remains a challenge, since no known algorithm produces a guaranteed survivable mapping. The design principle proposed in [19] provides a mapping that ensures the upper-layer topology connectivity in any single lower-layer link failure. In theory, upper-layer topology connectivity in all single lower-layer link failures does not necessarily guarantee the existence of lower-layer link-disjoint path pairs between any two upper-layer nodes [20]. Interested readers may refer to Fig. 3 in [20] for an illustrative example. However, references [3,21] and our

practice show that the latter property can be well satisfied using the principle in [19].

We illustrate a survivable mapping obtained from [19] for a simple example. A survivable mapping for the two-layer network in Fig. 1 is given in Table 1, and is represented by matrix Θ in (3).

$$\Theta = \begin{pmatrix} 1 & 0 & 0 & 0 & 0 & 0 & 0 \\ 0 & 1 & 0 & 0 & 0 & 1 & 0 \\ 0 & 1 & 0 & 0 & 0 & 0 & 1 \\ 0 & 0 & 1 & 0 & 0 & 0 & 0 \\ 0 & 0 & 0 & 1 & 0 & 0 & 1 \\ 0 & 0 & 0 & 0 & 1 & 0 & 0 \end{pmatrix} \begin{matrix} 1 \\ 2 \\ 3 \\ 4 \\ 5 \\ 6 \end{matrix} \quad (3)$$

3.2. Our proposed flow availability model

As we assume that link failures are mutually independent at the lower layer, we propose to find out the set of lower-layer links used by an upper-layer path, and build a flow availability model at the lower layer.

Each flow $s \in \mathcal{D}_u$ maintains on the upper-layer topology a working path $\sigma^s = \{\sigma_j^s\}_{1 \times |\mathcal{L}_u|}$ and a backup path $\tau^s = \{\tau_j^s\}_{1 \times |\mathcal{L}_u|}$, where the j -th element of the vectors equals one if the path traverses upper-layer link j ; equals zero otherwise. We denote the lower-layer layout of working path σ^s and backup path τ^s by binary row vectors $\rho^s = \{\rho_i^s\}_{1 \times |\mathcal{L}_l|}$ and $\zeta^s = \{\zeta_i^s\}_{1 \times |\mathcal{L}_l|}$, respectively, where the

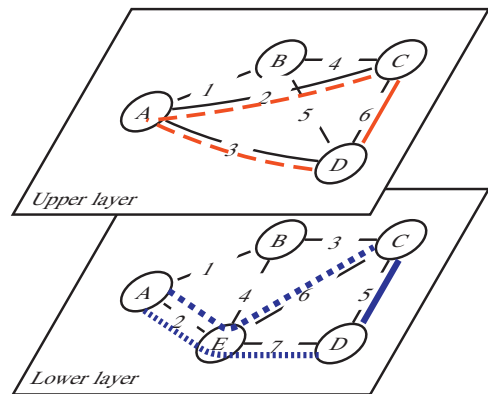


Fig. 1. Illustration of dedicated path protection at the upper layer. The number marked on a link indicates the link index. (For interpretation of the references to color in this figure caption, the reader is referred to the web version of this paper.)

Table 1
A survivable mapping for the two-layer network in Fig. 1.

Upper-layer link	Lower-layer path
1 (A-B)	A-B
2 (A-C)	A-E-C
3 (A-D)	A-E-D
4 (B-C)	B-C
5 (B-D)	B-E-D
6 (C-D)	C-D

i -th element equals one if the corresponding path traverses lower-layer link i at least once; equals zero otherwise. Note that a working or a backup path can traverse a lower-layer link multiple times [22]. An example is given in Fig. 1, where a flow is routed on the upper-layer topology with C–D as the working path (red solid line) and C–A–D as the backup path (red dashed line). Considering the link mapping in (3), the actual routing of the working and the backup paths on the lower-layer topology is C–D (blue solid line) and C–E–A–E–D (blue dashed line), respectively, where the backup path traverses lower-layer link A–E twice. The key information that vectors ρ^s and ζ^s capture is whether or not a given lower-layer link is used by the working or the backup path, regardless of how many times the lower-layer link is traversed. Consequently, elements ρ_i^s and ζ_i^s can be computed, respectively, as

$$\rho_i^s = u \left(\sum_{j \in \mathcal{L}_u} \sigma_j^s \theta_{ji} \right), \quad i \in \mathcal{L}_l, s \in \mathcal{D}_u, \quad (4)$$

and

$$\zeta_i^s = u \left(\sum_{j \in \mathcal{L}_u} \tau_j^s \theta_{ji} \right), \quad i \in \mathcal{L}_l, s \in \mathcal{D}_u, \quad (5)$$

where $\sum_{j \in \mathcal{L}_u} \sigma_j^s \theta_{ji}$ and $\sum_{j \in \mathcal{L}_u} \tau_j^s \theta_{ji}$ calculate the number of times the corresponding path traverses link i , and $u(x)$ is a step function defined as

$$u(x) = \begin{cases} 1 & \text{if } x \geq 1, \\ 0 & \text{if } x < 1, \end{cases} \quad (6)$$

which equals one when argument x is no less than one, and equals zero otherwise.

The failure independence on lower-layer links together with the lower-layer link-disjointness of working and backup paths enable simple flow availability formulations using the series-parallel method. The series-parallel method is suitable when a system can be characterized by a combination of mutually independent serially and/or parallelly structured subsystems, with each subsystem further consisting of independent components. A serially structured subsystem fails if any one of its components fails. In contrast, a parallelly structured subsystem fails only if all of its components fail. Our availability model for flow s is given in Fig. 2(a) using a series-parallel block diagram. Availability of working and backup paths of flow s is computed, respectively, as

$$A_s^{u,w} = \prod_{i \in \mathcal{L}_l} A_i^{\rho_i^s} = \prod_{i \in \mathcal{L}_l} A_i^{u(\sum_{j \in \mathcal{L}_u} \sigma_j^s \theta_{ji})}, \quad s \in \mathcal{D}_u, \quad (7)$$

and

$$A_s^{u,p} = \prod_{i \in \mathcal{L}_l} A_i^{\zeta_i^s} = \prod_{i \in \mathcal{L}_l} A_i^{u(\sum_{j \in \mathcal{L}_u} \tau_j^s \theta_{ji})}, \quad s \in \mathcal{D}_u, \quad (8)$$

where superscripts “ u,w ” and “ u,p ” refer to working and backup paths at the upper layer, respectively.

The property of lower-layer link-disjointness of the working and backup paths can be formulated as

$$\rho_i^s + \zeta_i^s \leq 1, \quad i \in \mathcal{L}_l, s \in \mathcal{D}_u. \quad (9)$$

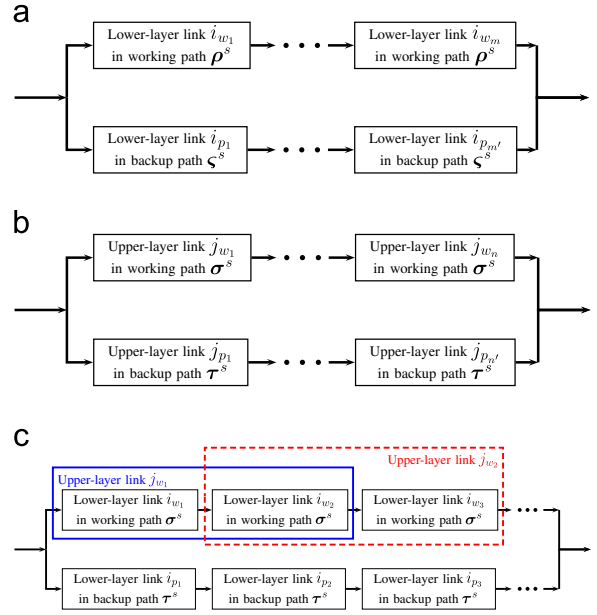


Fig. 2. Series-parallel diagram for flow availability calculation when protection is deployed at the upper layer. (a) Proposed flow availability model. (b) Existing flow availability model. (c) Problem with the existing flow availability model.

Then, unavailability of flow s is given by

$$U_s^{u,f} = (1 - A_s^{u,w})(1 - A_s^{u,p}), \quad s \in \mathcal{D}_u, \quad (10)$$

where superscript “ u,f ” refers to an upper-layer flow.

4. Flow availability model for protection at the lower layer

4.1. Our proposed flow availability model

When protection is deployed at the lower layer, each upper-layer link j is physically laid out as a working lower-layer path $\mu^j = \{\mu_i^j\}_{1 \times |\mathcal{L}_l|}$ and a link-disjoint backup lower-layer path $\nu^j = \{\nu_i^j\}_{1 \times |\mathcal{L}_l|}$. The i -th element of the vectors equals one if the lower-layer path traverses lower-layer link i ; equals zero otherwise. As an illustrative example, we provide a simple two-layer network in Fig. 3, where upper-layer links A–B and B–D use lower-layer paths A–B and B–D as their working paths, respectively, with paths A–C–D–B and B–A–C–D as their corresponding backup paths.

We model the flow availability using the state-space modeling method, which partitions network states according to lower-layer link failure scenarios. Each network state corresponds to one lower-layer failure scenario, where certain lower-layer links are down. The occurrence of failure scenarios is mutually exclusive to ensure that network states do not have overlaps in failure events as shown in Fig. 4. Hence, the unavailability of a flow is computed as the sum of the probabilities of network states in which the flow is disrupted. Compared with protection at the upper-layer and our proposed model described in Section 3, protection at the lower layer cannot be efficiently modeled using the series-

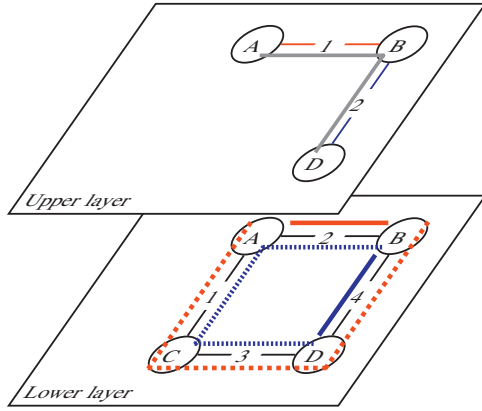


Fig. 3. Illustration of dedicated path protection at the lower layer.

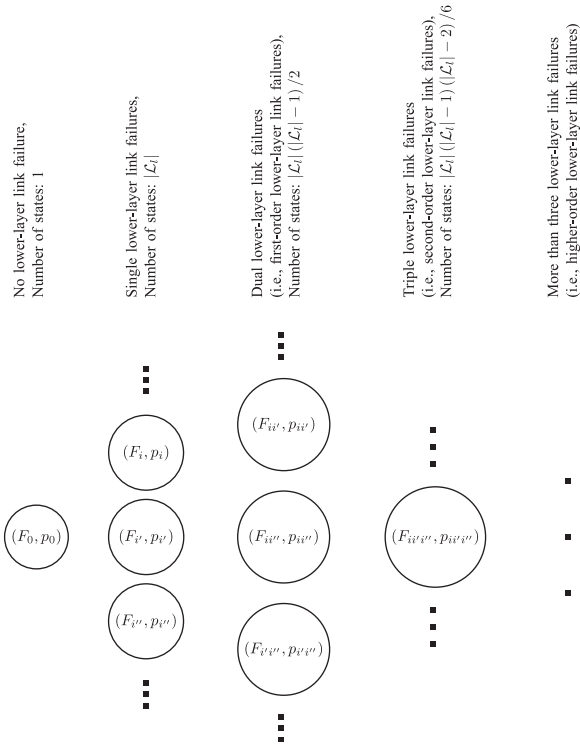


Fig. 4. Lower-layer link failure states considered in the state-space method for flow availability modeling when protection is deployed at the lower layer.

parallel method, and requires a more complicated modeling and approximation method.

We employ the state-space method to derive the proposed flow unavailability model by collecting network state probabilities at the lower layer up to triple lower-layer link failures. As it is computationally intractable to enumerate all possible network states (i.e., failure scenarios), a set of predominant network states with no more than three lower-layer link failures is considered instead based on the fact that probabilities of higher-order lower-layer failures (i.e., failures of more than three lower-layer links) are negligible. Our numerical results indicate that

considering only dual lower-layer link failures, which are the first-order failure events to cause flow outages, are not sufficient in unavailability calculation. Also note that in single lower-layer failure states, dedicated path protection at the lower layer ensures the upper-layer flows to be available.

Let $F_{ii'}$ denote the network state that two lower-layer links i and i' ($> i$) are down, and the rest of the lower-layer links are up. The state probability of $F_{ii'}$ is given by

$$p_{ii'} = U_i U_{i'} \prod_{i'' \in \mathcal{L}_l \wedge i'' \neq i, i'} A_{i''}, \quad i, i' \in \mathcal{L}_l, i < i'. \quad (11)$$

Upper-layer link j fails in state $F_{ii'}$ when one of links i and i' is on the working lower-layer path and the other on the backup lower-layer path. Let $\phi_{ii'}^j$ be a binary indicator, which equals one if upper-layer link j fails in state $F_{ii'}$; equals zero otherwise. Thus, $\phi_{ii'}^j$ is calculated as

$$\phi_{ii'}^j = \mu_i^j \nu_{i'}^j + \nu_i^j \mu_{i'}^j, \quad j \in \mathcal{L}_u, i, i' \in \mathcal{L}_l, i < i'. \quad (12)$$

For triple lower-layer link failures, similar notations are introduced. Let $F_{ii'i''}$ denote the network state that three lower-layer links i , i' ($> i$) and i'' ($> i'$) are down, and the other lower-layer links are up. The state probability of $F_{ii'i''}$ is given by

$$p_{ii'i''} = U_i U_{i'} U_{i''} \prod_{i''' \in \mathcal{L}_l \wedge i''' \neq i, i', i''} A_{i'''}, \quad i, i', i'' \in \mathcal{L}_l, i < i' < i''. \quad (13)$$

Let $\phi_{ii'i''}^j$ be a binary indicator, which equals one if upper-layer link j fails in state $F_{ii'i''}$; equals zero otherwise. Indicator $\phi_{ii'i''}^j$ is calculated as

$$\phi_{ii'i''}^j = u(\mu_i^j + \mu_{i'}^j + \mu_{i''}^j) \cdot u(\nu_i^j + \nu_{i'}^j + \nu_{i''}^j), \quad j \in \mathcal{L}_u, i, i', i'' \in \mathcal{L}_l, i < i' < i'', \quad (14)$$

where $\phi_{ii'i''}^j$ equals one when one of the three lower-layer links i , i' and i'' is on the working path of upper-layer link j , and another one of them is on the backup path of link j ; equals zero otherwise.

When protection is enabled at the lower layer, each flow s only maintains a working path σ^s at the upper layer. To compute the flow unavailability with protection at the lower layer and no protection at the upper layer, we identify the network states, where flow s is down. Let $\varphi_{ii'}^s$ denote a binary indicator, which equals one if flow s is disrupted in network state $F_{ii'}$; equals zero otherwise. We have

$$\varphi_{ii'}^s = u\left(\sum_{j \in \mathcal{L}_u} \sigma_j^s \phi_{ii'}^j\right), \quad s \in \mathcal{D}_u, i, i' \in \mathcal{L}_l, i < i', \quad (15)$$

where $\sum_{j \in \mathcal{L}_u} \sigma_j^s \phi_{ii'}^j$ counts the number of upper-layer links of flow s that fails in state $F_{ii'}$, and $u(x)$ is the step function defined in (6) to ensure that indicator $\varphi_{ii'}^s$ equals one if one or more upper-layer links of flow s fails in state $F_{ii'}$; equals zero otherwise. For example, in Fig. 3, both of the upper-layer links A–B and B–D of flow 1, which is routed along path A–B–D on the upper-layer topology, fail in dual-failure state F_{24} .

Similarly, we introduce binary indicator $\varphi_{ii'i''}^s$, which equals one if flow s is down in network state $F_{ii'i''}$; equals

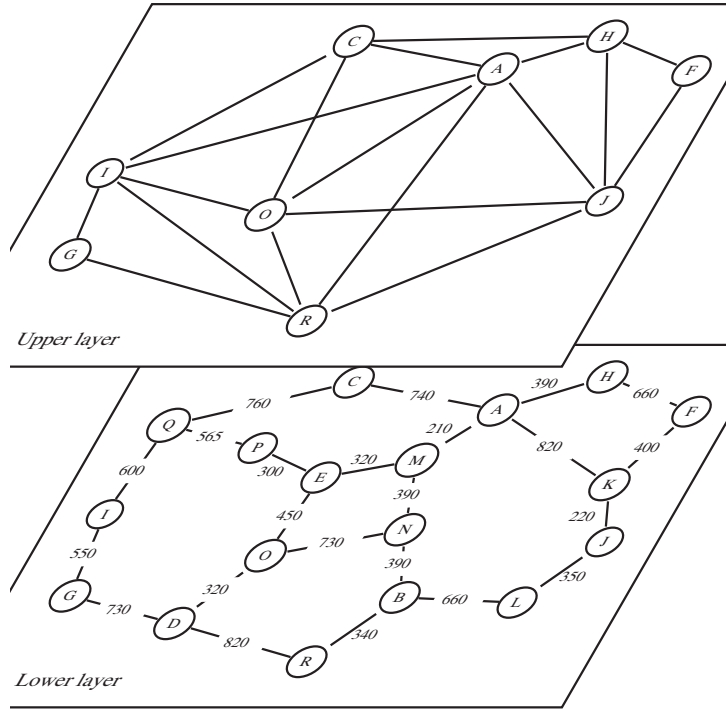


Fig. 5. Net 1 with 9 upper-layer nodes, 19 upper-layer links, 18 lower-layer nodes, and 23 lower-layer links.

zero otherwise. Indicator $\varphi_{ii''}^s$ is given by

$$\varphi_{ii''}^s = u \left(\sum_{j \in \mathcal{L}_u} \sigma_j^s \phi_{ii''}^j \right), \quad s \in \mathcal{D}_u, i, i'' \in \mathcal{L}_l, i < i'' \quad (16)$$

In Fig. 3 as an example, both of the upper-layer links A–B and B–D of flow 1 fail in triple-failure states F_{124} , and F_{234} .

We estimate the unavailability of flow s as the sum of the state probabilities that flow s is down, i.e.,

$$U_s^{u,f} = \sum_{i \in \mathcal{L}_l} \sum_{i' \in \mathcal{L}_l \wedge i' > i} p_{ii'} \cdot \varphi_{ii'}^s + \sum_{i \in \mathcal{L}_l} \sum_{i' \in \mathcal{L}_l \wedge i' > i'' \in \mathcal{L}_l \wedge i'' > i'} p_{ii''} \cdot \varphi_{ii''}^s, \quad s \in \mathcal{D}_u, \quad (17)$$

where the first and the second terms on the right side of the formula consider the contributions of dual and triple lower-layer link failures, respectively. We ignore states for higher-order failures of more than three lower-layer links.

4.2. Upper bound of flow unavailability

Strictly speaking, the proposed model in the previous subsection provides a lower bound on flow unavailability due to the truncation of more than three lower-layer link failures. In certain cases, we are also interested in obtaining a worst-case upper bound on flow unavailability, which can be approximated by using the following proposed method.

The upper bound on unavailability of flow s , denoted by $\bar{U}_s^{u,f}$, can be estimated by adding the probability of quadruple or more lower-layer link failures into the computed

unavailability $U_s^{u,f}$. This is a worst-case upper bound since we assume that any quadruple or more lower-layer link failure causes outage of flow s . In other words,

$$\bar{U}_s^{u,f} = U_s^{u,f} + P^{3+}, \quad s \in \mathcal{D}_u, \quad (18)$$

where P^{3+} denotes the probability of network states with quadruple or more lower-layer link failures. P^{3+} can be computed as

$$P^{3+} = 1 - p_0 - \sum_{i \in \mathcal{L}_l} p_i - \sum_{i \in \mathcal{L}_l} \sum_{i' \in \mathcal{L}_l \wedge i' > i} p_{ii'} - \sum_{i \in \mathcal{L}_l} \sum_{i' \in \mathcal{L}_l \wedge i' > i'' \in \mathcal{L}_l \wedge i'' > i'} p_{ii''}, \quad (19)$$

where p_0 denotes the probability of network state F_0 that all lower-layer links are up, and p_i denotes the probability of network state F_i that lower-layer link i is down, and all the other lower-layer links are up. Probabilities of network states F_0 and F_i are given, respectively, by

$$p_0 = \prod_{i \in \mathcal{L}_l} A_i, \quad (20)$$

and

$$p_i = U_i \prod_{i' \in \mathcal{L}_l \wedge i' \neq i} A_{i'}, \quad i \in \mathcal{L}_l. \quad (21)$$

5. Numerical results

5.1. Simulation settings

We use two example networks to evaluate the accuracy of flow availability estimations given by the proposed and

the existing analytical models. The example networks, Net 1 and Net 2, are shown in Figs. 5 and 6, respectively. The average nodal degrees of the lower-layer topologies are 2.56 and 3.65 for Net 1 and Net 2, respectively. Link lengths in km are marked on the lower-layer topologies. As the typical average nodal degree for carrier networks is 2.7 [23], results on Net 1 can have more practical relevance.

We vary the failure rates of lower-layer links to test the performance of the proposed flow availability model. Time to failure and failure repair time of each lower-layer link follow negative exponential distributions as assumed in Section 2. The mean failure rate of a link is measured in FIT/km, where 1 FIT (failure in time) refers to 1 failure in 10^9 h. When the link failure rate is 500 FIT/km, the MTTF of lower-layer networks is 170.7 h and 68.5 h for Net 1 and Net 2, respectively. The mean time to repair of a lower-layer link is assumed to be 12 h. We simulate flow unavailability under various link unavailability (i.e., link failure probabilities) using a discrete-event simulator written in OPNET. The unavailability of a flow is computed as the accumulated outage time divided by the total simulation time. Different link unavailability is set by varying the link failure rates. According to (1), this is equivalent to varying the MTTR of links adopted in [8,10]. We simulate the average flow unavailability up to a bit over 10^{-3} as service providers usually work with flow unavailability below 10^{-3} (i.e., availability of over “three nines”). The corresponding link failure rates are in the range of several hundred FIT/km, which is on the same order of link failure rate (312 FIT/km) observed in long-haul networks according to Telcordia statistics [24].

In our simulation, lower-layer links can fail with arbitrary combination and of arbitrary order. This is unlike the simulation method used in [9], which only collects the outage time of dual-link failures, and ignores the impact of more than two lower-layer links. In our simulation, all possible failure scenarios that disrupt a flow are counted in the outage time of the flow.

5.2. Flow availability with protection at the upper layer

We obtain a mapping of upper-layer links to lower-layer paths using the link-path version of the ILP model proposed in [19]. The link-path formulation can be found in [25]. For each upper-layer link, we feed into the ILP model up to 50 pre-calculated candidate paths, which are generated by using the K shortest path algorithm based on the lower-layer hop count metric.

We enumerate various path pairs for each upper-layer node pair so that many possible routing solutions are taken into consideration, and study the average unavailability performance without being dominated by a small number of particular path pairs. For each upper-layer node pair, 5 working paths and 5 lower-layer link-disjoint backup paths associated with each working path are computed on the upper-layer topologies, if they exist, by using the K shortest path algorithm. The lower-layer hop counts of upper-layer links are used as link costs on the upper-layer topologies. The total numbers of flows calculated are 601, i.e., $|\mathcal{D}_u| = 601$, for Net 1, and 821, i.e., $|\mathcal{D}_u| = 821$, for Net 2.

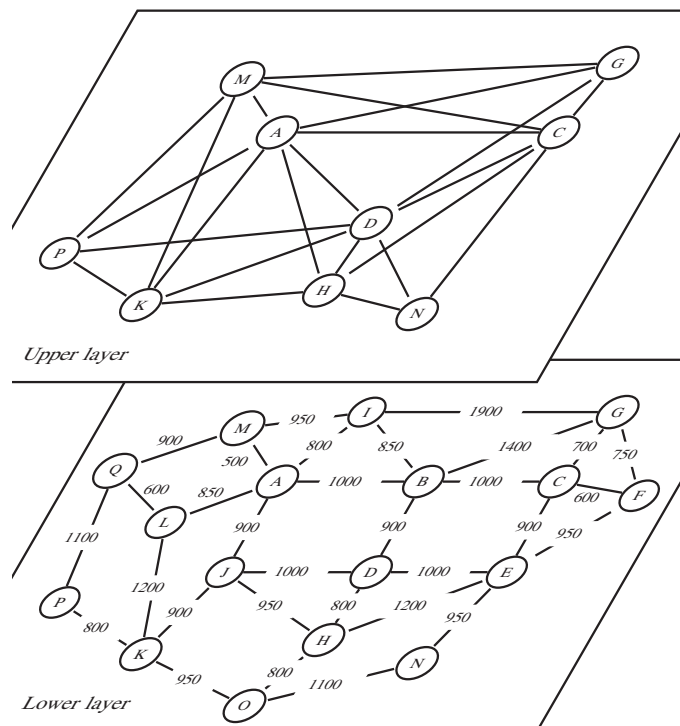


Fig. 6. Net 2 with 9 upper-layer nodes, 23 upper-layer links, 17 lower-layer nodes, and 31 lower-layer links.

5.2.1. Number of flows with overestimated unavailability

We identify flows with either working or backup path traversing any lower-layer link more than once as “multi-crossing flows”, denoted by set

$$\mathcal{M}_u = \left\{ s \in \mathcal{D}_u \mid i \in \mathcal{L}_l : \sum_{j \in \mathcal{L}_u} \sigma_j^s \theta_{ji} > 1 \vee \sum_{j \in \mathcal{L}_u} \tau_j^s \theta_{ji} > 1 \right\}. \quad (22)$$

The sizes of the flow sets are summarized in Table 2. The size of set \mathcal{M}_u is found to be 400, which is around 66.6% of the total flows, for Net 1, and 257, which is around 31.3% of the total flows, for Net 2. The proportion of total flows included in set \mathcal{M}_u , i.e., $|\mathcal{M}_u|/|\mathcal{D}_u|$, on Net 1 is much larger than that on Net 2 due to the sparser lower-layer topology of Net 1 than that of Net 2. A sparser lower-layer topology limits link mapping diversity, and causes more overlapped mapping of upper-layer links on lower-layer links. As a result, upper-layer paths are more likely to use lower-layer links more than once. For flows outside of set \mathcal{M}_u , i.e., $\mathcal{D}_u \setminus \mathcal{M}_u$, there is no overestimation of unavailability. We focus on flows in set \mathcal{M}_u to compare the accuracy of the existing and the proposed availability models.

5.2.2. Extent of flow unavailability overestimation

We compare average flow unavailability obtained from our proposed model and the existing model in [12–14] with simulation results. Figs. 7 and 8 show the average unavailability on Net 1 and Net 2, respectively. The data are taken over all the flows in set \mathcal{M}_u . We see that our proposed model fits well with the simulation results: nearly all the analytical results fall into the 95% confidence intervals of the simulation results for Net 1; and all are within the intervals for Net 2. This confirms the accuracy of our proposed model. On the contrary, the model in [12–14] gives much higher average unavailability than the simulation results for both networks because set \mathcal{M}_u is formed by flows with overestimated unavailability given by the existing model. More specifically, the existing model builds flow availability upon the availability of upper-layer links by assuming independent upper-layer link failures. The associated series-parallel diagram is given in Fig. 2(b). However, since different upper-layer links can share the same lower-layer link, if an upper-layer path traverses a lower-layer link multiple times as shown in Fig. 2(c), the availability of the lower-layer link is counted the same number of times in the existing model, and thus overbuilds the value of path unavailability. Consequently, flow unavailability as a product of working and backup path unavailability is

Table 2
Percentage of multi-crossing flows in total flows for protection at the upper layer.

Example network	Total flows, i.e., $ \mathcal{D}_u $	Number of multi-crossing flows, i.e., $ \mathcal{M}_u $	Percentage of multi-crossing flows in total flows, i.e., $ \mathcal{M}_u / \mathcal{D}_u \times 100\%$
Net 1	601	400	66.6
Net 2	821	257	31.3

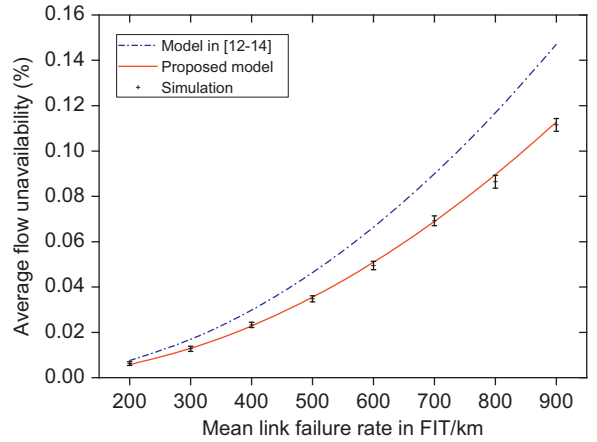


Fig. 7. Average unavailability of multi-crossing flows on Net 1 with dedicated path protection at the upper layer.

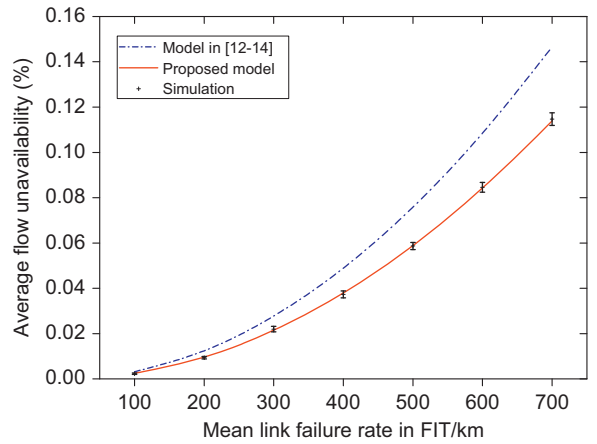


Fig. 8. Average unavailability of multi-crossing flows on Net 2 with dedicated path protection at the upper layer.

overestimated when any one of the two paths traverses a lower-layer link more than once.

As a quantitative metric to characterize the overestimation of flow unavailability in the existing model in [12–14], we define the unavailability overbuild of flow s as

$$O_s^{u,f} = \frac{\tilde{U}_s^{u,f} - U_s^{u,f}}{U_s^{u,f}} \times 100\%, \quad s \in \mathcal{M}_u, \quad (23)$$

where $\tilde{U}_s^{u,f}$ and $U_s^{u,f}$ denote the flow unavailability computed by the existing model and by our proposed model, respectively. We observe that the average unavailability overestimation is significant on both networks shown in Fig. 9. For all the lower-layer link failure rates studied, the average overbuild is constantly around 30% on Net 1 and is around 28% on Net 2.

5.2.3. Distribution of flow unavailability overestimation

Fig. 10 takes a snapshot of the unavailability of individual multi-crossing flows on Net 1. Link failure rate is set to 600 FIT/km. We count the numbers of flows that

are below, within, and above the 95% confidence ranges for both models. The comparative results between our proposed model and the model in [12–14] are 2 vs. 0 for below the ranges, 374 vs. 36 for within the ranges, and 24 vs. 364 for above the ranges. We observe a significant improvement of our proposed model over the model in [12–14] in terms of per-flow unavailability accuracy. Taking the flows in set $\mathcal{D}_u \setminus \mathcal{M}_u$ into account, Fig. 12 shows the proportions of all flows that are within, above, and below the 95% confidence ranges. The comparative results between our proposed model and the model in [12–14] are 90.4% vs. 34.1% for within the ranges, 9.3% vs. 65.9% for above the ranges, and 0.3% vs. 0% for below the ranges.

Similar improvement is also observed in Fig. 11, which takes a snapshot of the unavailability of multi-crossing flows on Net 2. Link failure rate is 400 FIT/km. We find that with the model in [12–14], only 6 flows are within the confidence intervals. The majority of 251 flows fall out of the ranges with higher unavailability values. In contrast, by using our proposed model, unavailability of 249

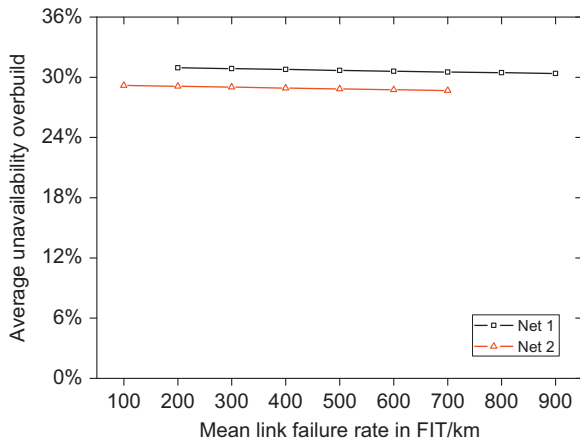


Fig. 9. Average unavailability overbuild of multi-crossing flows with dedicated path protection at the upper layer.

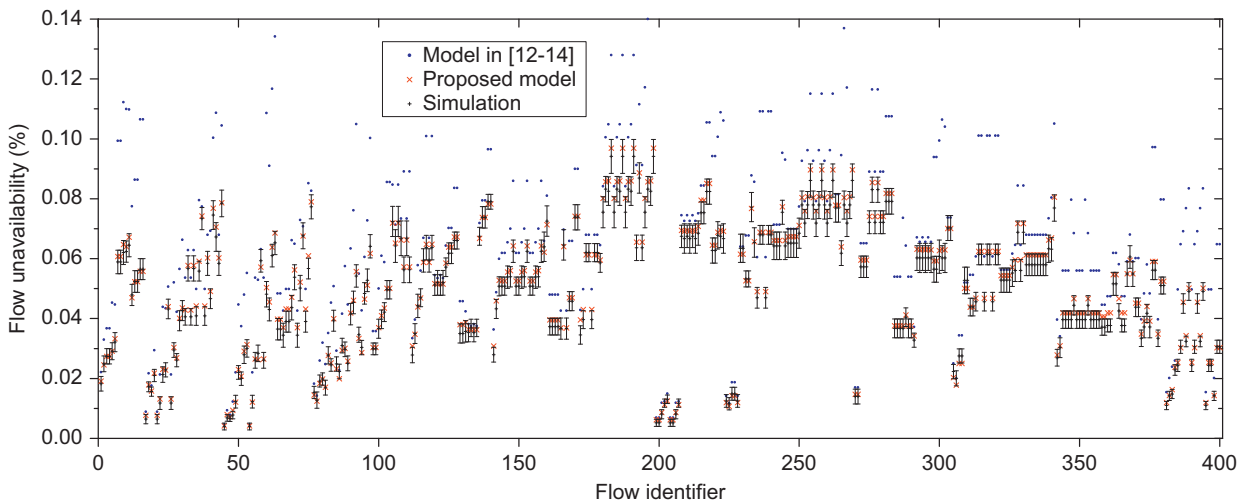


Fig. 10. Unavailability of multi-crossing flows on Net 1 with dedicated path protection at the upper layer and link failure rate of 600 FIT/km.

flows falls within the 95% confidence intervals, and only 8 flows are above the confidence ranges. This again indicates the accuracy gain of our proposed model over the existing model in [12–14]. Fig. 13 shows a complete picture of the proportions of all flows (i.e., flows in set \mathcal{D}_u) that are within, above, and below the 95% confidence intervals. The comparative results between our proposed model and the model in [12–14] are 94.8% vs. 65.2% for within the intervals, 5.2% vs. 34.8% for above the intervals, and 0% vs. 0% for below the intervals.

5.3. Flow availability with protection at the lower layer

In the case of protection at the lower layer, each upper-layer link is laid out as a pair of link-disjoint lower-layer paths with minimum lower-layer hop counts. Such a path pair is found through the link-disjoint shortest pair algorithm in [26], which has polynomial computational complexity.

When the lower-layer path pair for each upper-layer link is found, 10 shortest single paths per upper-layer node pair are computed on the upper-layer topology using the K shortest path algorithm with hop counts of lower-layer path pairs serving as the upper-layer link costs. The total numbers of flows generated on Net 1 and Net 2 are both 360. These flows form sets \mathcal{D}_u on the corresponding networks.

5.3.1. Number of flows with overestimated unavailability

Among the generated flows under study, we further identify the flows that have multiple (≥ 2) upper-layer links disrupted in the same dual-lower-layer-link-failure state(s) as “multi-crossing flows”, denoted by set

$$\mathcal{Q}_u = \left\{ s \in \mathcal{D}_u \mid i, i' \in \mathcal{L}_u, i < i' : \sum_{j \in \mathcal{L}_u} \sigma_j^s \phi_{ii'}^j > 1 \right\}. \quad (24)$$

Note that in (24) we use the first-order dual-failure network states to select flows as numerical results show that redundancy that exists only among the second-order

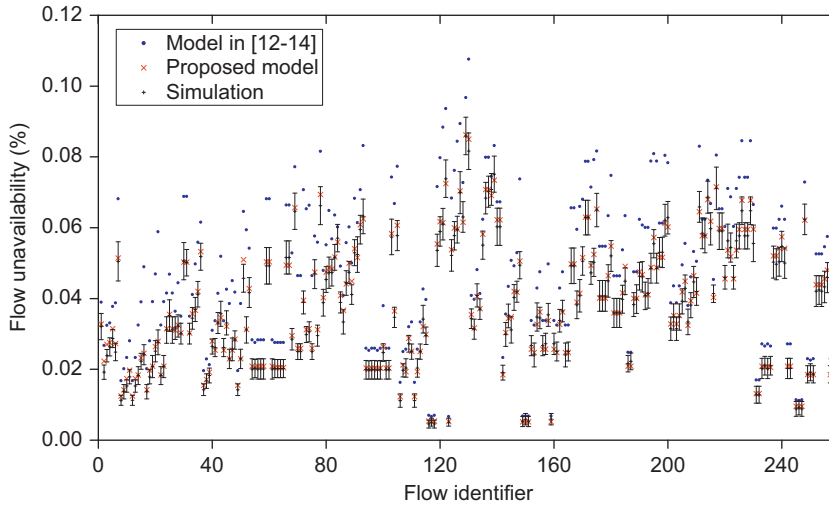


Fig. 11. Unavailability of multi-crossing flows on Net 2 with dedicated path protection at the upper layer and link failure rate of 400 FIT/km.

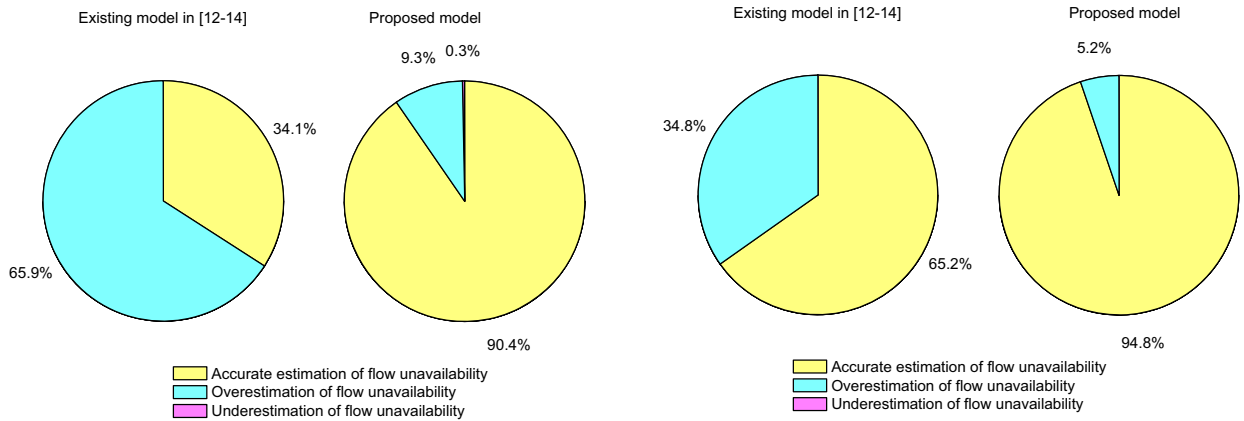


Fig. 12. Proportion of all flows within, above, and below the 95% confidence intervals of the simulation results on Net 1 with link failure rate of 600 FIT/km and dedicated path protection at the upper layer.

Fig. 13. Proportion of all flows within, above, and below the 95% confidence intervals of the simulation results on Net 2 with link failure rate of 400 FIT/km and dedicated path protection at the upper layer.

triple-failure states has marginal effects on unavailability calculation accuracy. The sizes of the flow sets are summarized in Table 3. The set size of Q_u is 321, which is around 89.2% of the total flows, on Net 1, and is 112, which is around 31.1% of the total flows, on Net 2. The proportion of total flows involved in set Q_u , i.e., $|Q_u|/|D_u|$, on Net 1 turns out to be much higher than that on Net 2. Similar to the case of protection at the lower layer, this can be explained by the sparser lower-layer topology of Net 1 than that of Net 2. A sparser lower-layer topology greatly reduces the diversity of link-disjoint lower-layer path pairs. Hence, when the upper-layer links are laid out in the form of lower-layer path pairs, they are more intertwined on the lower-layer topology. Consequently, upper-layer flows enjoy a much higher probability of having multiple traversed upper-layer links failing in the same lower-layer dual-failure states. For tidiness, we do not show the availability results for flows in set $D_u \setminus Q_u$, but we confirm that though using different calculation methods, flow unavailability computed by our model and

Table 3
Percentage of multi-crossing flows in total flows for protection at the lower layer.

Example network	Total flows, i.e., $ D_u $	Number of multi-crossing flows, i.e., $ Q_u $	Percentage of multi-crossing flows in total flows, i.e., $ Q_u / D_u \times 100\%$
Net 1	360	321	89.2
Net 2	360	112	31.1

by the model in [12–14] are closely approximate to each other, and agree well with the simulation results on both networks. In the following, we focus on the flows in set Q_u to compare the proposed and the existing models.

5.3.2. Extent of flow unavailability overestimation

Figs. 14 and 15 show the average unavailability taken over all the flows in set Q_u on Net 1 and Net 2, respectively. Comparing the curves of the existing model [12–14] with the simulation results, we see that results

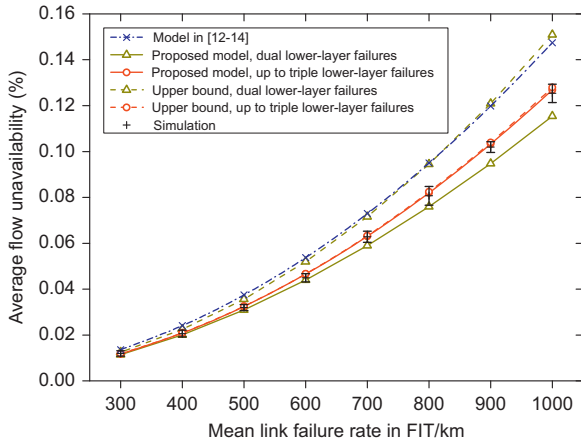


Fig. 14. Average unavailability of multi-crossing flows on Net 1 with dedicated path protection at the lower layer.

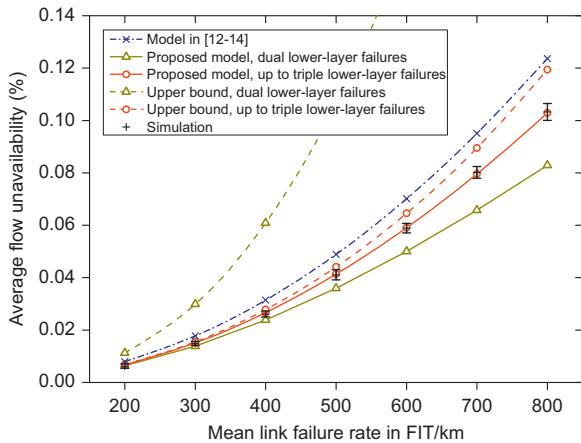


Fig. 15. Average unavailability of multi-crossing flows on Net 2 with dedicated path protection at the lower layer.

given by [12–14] all fall above the 95% confidence intervals of the simulation results. This is because set Q_u is composed of flows that have unavailability overestimation with the existing model in [12–14], which relies on the availability of upper-layer links and the implicit assumption of independent upper-layer link failures to approximate the flow availability. However, if multiple upper-layer links of a flow fail in the same network state, probability of the network state contributes to the flow unavailability multiple times, thus leading to redundant calculations by using the existing model. On the other hand, when we use the proposed model to compute the flow unavailability, we find that the results are very close to the simulation results with all the average values falling within the 95% confidence intervals. The accuracy of our proposed model comes from the removal of redundant unavailability calculations caused by the existing model.

To further quantify the calculation redundancy of the existing unavailability model in [12–14], we use the unavailability overbuild metric defined in (23), where set \mathcal{M}_u is replaced by set Q_u for the current context.

Clearly, a higher unavailability overbuild indicates more redundancy computed by the existing model [12–14]. In Fig. 16, we observe considerable average unavailability overbuild on both networks. On Net 1, the average overbuild is above 15% under all lower-layer link failure rates, and increases slowly as the failure rate gets higher. Turning to Net 2, we see a similar increasing trend, but at a more rapid pace. Specifically, moving from the link failure rate of 200 FIT/km to 800 FIT/km, the average unavailability overbuild increases from 17.1% to 20.2% accordingly.

5.3.3. Justification of considering up to triple lower-layer link failures

To justify the necessity of introducing triple lower-layer link failures in unavailability calculations, we include in Figs. 14 and 15 the average flow unavailability curves computed by the proposed model which, however, only considers dual-lower-layer-link-failure states. For Net 1, we see that when link failure rates are not greater than 600 FIT/km, calculations with dual-failure states are still within the 95% confidence intervals of the simulation results, but all of the computed values are below the mean simulated values, and deviate more from the mean simulated values as the failure rate increases. When the link failure rate reaches 700 FIT/km and beyond, calculations with dual failures go below the confidence ranges, and the gap to the simulation results becomes larger. The above trend indicates that unavailability calculations considering only dual-lower-layer-link-failure states can be accurate when the link failure rate is low enough to the extent that contributions of dual failures to flow unavailability are dominant while the contributions of triple failures are negligible. However, when the link failure rate is high in the sense that contributions of dual failures and triple failures to flow unavailability become comparable, considering only dual failures in unavailability calculations becomes insufficient, and triple failures should be included in the proposed model accordingly as in (17). A similar trend is also observed on Net 2 with a magnified effect. Specifically, calculation with dual

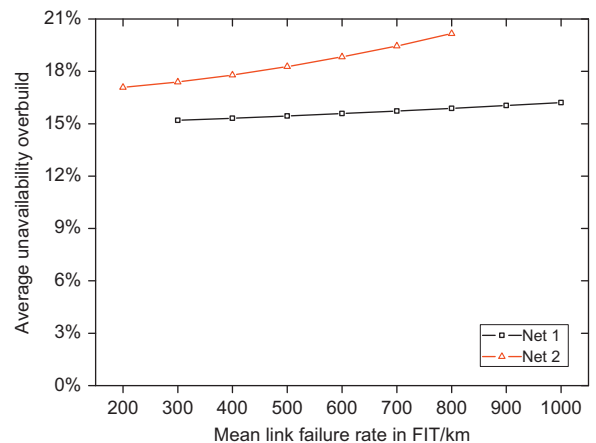


Fig. 16. Average unavailability overbuild of multi-crossing flows with dedicated path protection at the lower layer.

failures is only accurate at link failure rate of 200 FIT/km. For the rest of the failure rates studied (i.e., from 300 to 800 FIT/km), all of the calculations are far below the confidence ranges of the simulation results. This is because given the same link failure rate, the MTTF value of the lower-layer topology on Net 2 is much lower than that on Net 1 as discussed in the simulation settings. Or equivalently, to reach the same MTTF value of the lower-layer network, the link failure rate with Net 2 is much smaller than that with Net 1. Moreover, one can see in Fig. 15 that the disparity between the two results becomes larger with the increase of the link failure rate.

In short, both Figs. 14 and 15 show the need to include triple lower-layer failures in the proposed analytical model particularly as the link failure rate gets higher. On the other hand, we simulate the average flow unavailability up to over 10^{-3} , which corresponds to an average availability level of less than 0.999 (“three nines”). We see in both Figs. 14 and 15 that triple-failure coverage still works well for that unavailability range with negligible truncation errors. As service providers usually manage the flow unavailability to be no greater than 10^{-3} (corresponding to flow availability of no less than “three nines”) [5,27], we expect considering triple lower-layer link failures to be sufficient to deliver accurate calculations for practical unavailability concerns.

5.3.4. Upper bound on flow unavailability

Figs. 14 and 15 also plot the upper bounds on flow unavailability corresponding to our proposed models with only dual lower-layer link failures and with up to triple lower-layer link failures. Recall that our proposed model provides a lower bound on flow unavailability in the strict sense. We see that with only dual lower-layer failures, gaps between the two bounds (i.e., the upper and the lower bounds) as well as gaps between the upper bound and the simulation results are both large on two networks, particularly for Net 2. By including triple lower-layer failures in our proposed model, both gaps are narrowed. On Net 1, both gaps become negligible. The two bounds are almost identical to each other. This indicates a tight upper bound

on flow unavailability. On Net 2, both gaps are small when the network failure rate is low, but increase considerably as the network failure rate gets higher. In other words, the upper bound gets loose with the increase of the network failure rate. Moreover, we observe that flow unavailability given by the existing model is very close to the upper bound associated with our model considering only dual lower-layer link failures on Net 1, and is higher than the upper bound of our model with up to triple lower-layer link failures on Net 2.

5.3.5. Distribution of flow unavailability overestimation

Fig. 17 takes a snapshot of the unavailability of multi-crossing flows on Net 1 when link failure rate is 700 FIT/km. It is encouraging to find that all the flow unavailability computed by our model is within the 95% confidence intervals of the simulation results. In contrast, by using the model in [12–14], only 60 flows are within the confidence ranges while the other 261 flows have their unavailability overestimated with the values falling above the ranges. To give a complete view, Fig. 19 shows the proportions of all flows (i.e., flows in set \mathcal{D}_i) that are within, above, and below the 95% confidence intervals. The comparative results between our proposed model and the model in [12–14] are 100% vs. 27.5% for within the intervals, 0% vs. 72.5% for above the intervals, and 0% vs. 0% for below the intervals.

A snapshot of the unavailability of multi-crossing flows on Net 2 is given by Fig. 18. Link failure rate is set to 500 FIT/km. For both models, we count the number of flows whose unavailability values are below, within, and above the confidence intervals of the simulation results. The comparative results between our model and the model in [12–14] are 1 vs. 0 for below the intervals, 111 vs. 23 for within the intervals, and 0 vs. 89 for above the intervals. For flows whose unavailability values are within the confidence intervals using both models, we further calculate the percentage error between the approximation value of the analytical results and the mean value of the simulation results. The average percentage errors taken over these flows are 1.98% for our model

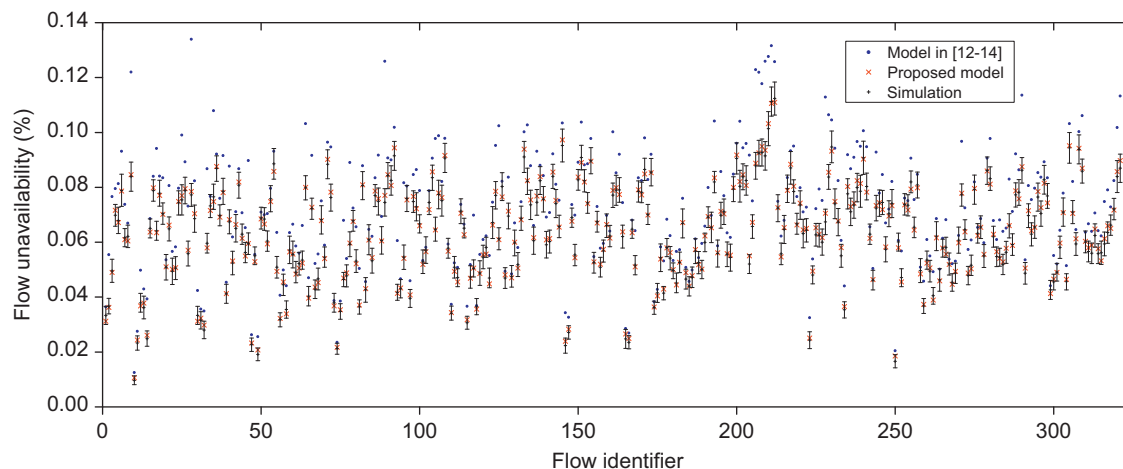


Fig. 17. Unavailability of multi-crossing flows on Net 1 with dedicated path protection at the lower layer and link failure rate of 700 FIT/km.

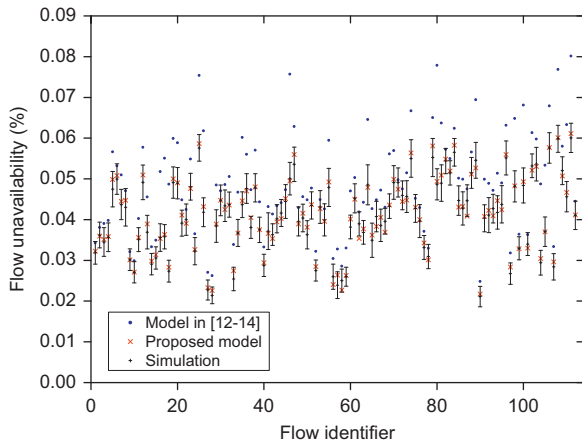


Fig. 18. Unavailability of multi-crossing flows on Net 2 with dedicated path protection at the lower layer and link failure rate of 500 FIT/km.

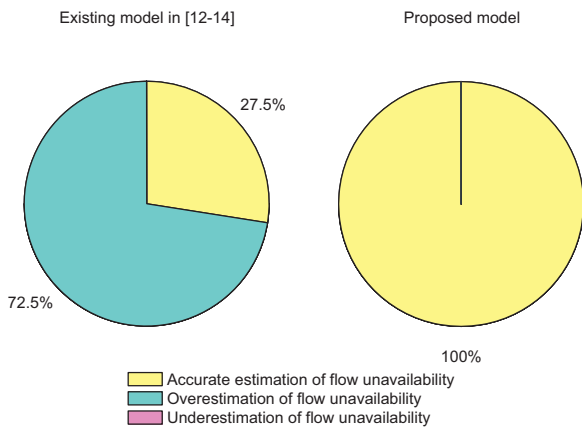


Fig. 19. Proportion of all flows within, above, and below the 95% confidence intervals of the simulation results on Net 1 with link failure rate of 700 FIT/km and dedicated path protection at the lower layer.

and 6.29% for the model in [12–14]. This means that even for the flows whose analytical results are both within the confidence intervals, our model matches the mean simulated value closer than the model in [12–14]. Next, for a complete picture, Fig. 20 shows the proportions of all flows (i.e., flows in set \mathcal{D}_u) that are within, above, and below the 95% confidence intervals. The comparative results between our proposed model and the model in [12–14] are 98.1% vs. 74.2% for within the intervals, 0% vs. 24.7% for above the intervals, and 1.9% vs. 1.1% for below the intervals.

The per-flow unavailability results in both Figs. 17 and 18 further show that our proposed model outperforms the existing model in [12–14] in terms of approximation accuracy.

5.4. Flow availability comparison between two protection schemes

Let us consider the following incremental network design situation: assume that all the existing flows in a two-layer carrier network are unprotected. Specifically,

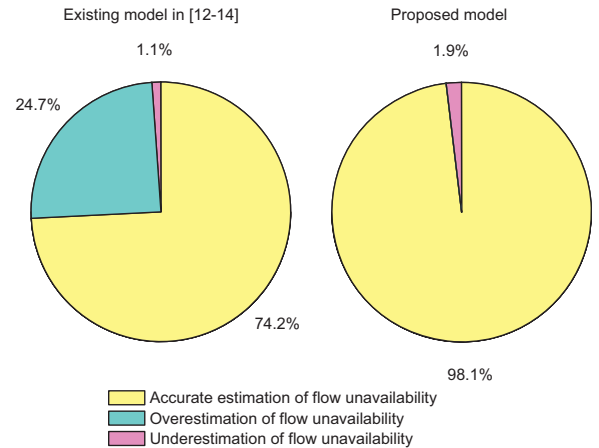


Fig. 20. Proportion of all flows within, above, and below the 95% confidence intervals of the simulation results on Net 2 with link failure rate of 500 FIT/km and dedicated path protection at the lower layer.

each logical link is laid out as a single lower-layer path, and each flow maintains a single path at the upper layer. Now the network carrier would like to protect all the flows by deploying in the network one and only one of the two protection schemes, i.e., protection at the upper layer or protection at the lower layer. An interesting question is: which protection scheme provides better average flow availability?

We perform case studies on Net 1 and 2. For each upper-layer node pair, we generate only one flow, which is routed over the shortest upper-layer path. The upper-layer link cost is chosen to be the corresponding lower-layer hop count. In the upper-layer protection scheme, a shortest backup path which is lower-layer link-disjoint with the working path is routed based on the same upper-layer link cost metric. In the case of lower-layer protection, a link-disjoint lower-layer path with the shortest hop count is routed to protect the working lower-layer path of each logical link.

Figs. 21 and 22 show on the left axes the average unavailability taken over all the flows on Net 1 and Net 2, respectively. We see that on both networks, the average flow unavailability with protection at the lower layer is lower than that with protection at the upper layer. This can be explained by the fact that replication at the component level (i.e., at the lower layer for the upper-layer links in our context) is more effective than replication at the system level (i.e., at the upper layer for the upper-layer paths) [28]. For reference, we plot the average unavailability of all the flows before protection on the right axes of the figures.

6. Conclusions

In this paper, we studied analytical models for flow availability in two-layer networks with dedicated path protection. Specifically, we considered two protection options, namely, protection at the upper layer, and protection at the lower layer. For both protection schemes, we proposed new models that build the flow unavailability

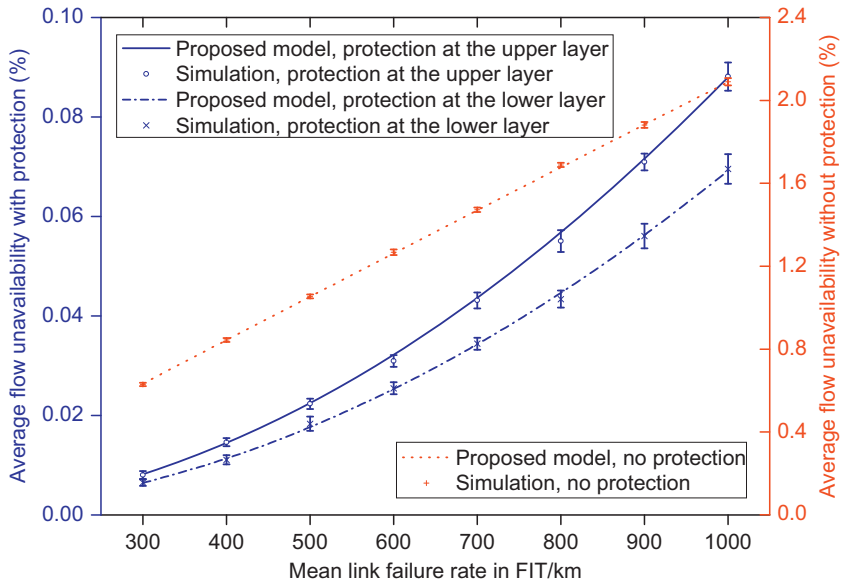


Fig. 21. Average flow unavailability on Net 1.

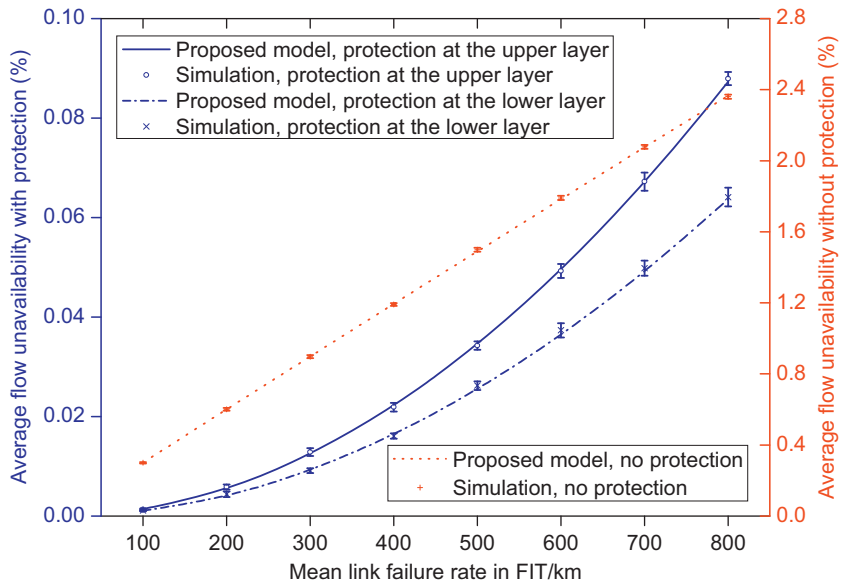


Fig. 22. Average flow unavailability on Net 2.

accurately at the lower layer, where link failures are mutually independent, so that redundant calculations are canceled out.

In simulation, we identify the flows whose unavailability is overestimated using the existing models, which compute the flow availability at the upper layer, where link failures are correlated, by implicitly assuming failure independence of upper-layer links. These identified flows constitute 31.3% to 66.6% and 31.1% to 89.2% of the total flows in the case of protection at the upper layer and protection at the lower layer, respectively. The proportion of the identified flows among the total flows shows a lower-layer-topology-dependence property. In particular,

the proportion tends to be higher when the lower-layer network topology becomes sparser.

Numerical results show that by using the existing models, only 2.3% to 9.0% of the identified flows have their unavailability values falling within the 95% confidence intervals of the simulation results when protection is deployed at the upper layer. In the case of protection at the lower layer, the percentage ranges from 18.7% to 20.5%. In contrast, when the proposed flow unavailability models are used to replace the existing ones, the corresponding percentages are improved significantly to over 93.5% for protection at the upper layer and to over 99.1% for protection at the lower layer. Moreover, even for the

flows with both of the analytical results falling within the confidence intervals, the analytical results of the proposed models match the mean simulated values closer than those of the existing models. To quantify the overestimation property of the existing models, the unavailability overbuild metric is introduced. Numerical results show that the average unavailability overbuild for protection at the upper layer and for protection at the lower layer is over 28% and over 15%, respectively. Last, we compared flow availability between the two protection schemes. Numerical results show that given the same initial unprotected network states, the average flow unavailability deploying lower-layer protection is smaller than that deploying upper-layer protection.

Acknowledgments

Dr. Ni is highly indebted to Prof.-Dr. D.A.A. Mello for his help in understanding his work and the availability topic in general, and to Prof.-Dr. M. Tornatore for discussions on his work. The authors would like to thank anonymous reviewers for their constructive comments to improve the paper. Dr. Jing Wu acknowledges the research support from the State Key Laboratory of Advanced Optical Communication Systems and Networks, Shanghai Jiao Tong University, China.

References

- [1] C. Ou, K. Zhu, J. Zhang, H. Zhu, B. Mukherjee, H. Zang, L.H. Sahasrabudde, Traffic grooming for survivable WDM networks: dedicated protection, *OSA Journal of Optical Networking* 3 (1) (2004) 40–74.
- [2] C. Ou, K. Zhu, H. Zang, L.H. Sahasrabudde, B. Mukherjee, Traffic grooming for survivable WDM networks—shared protection, *IEEE Journal on Selected Areas in Communications* 21 (9) (2003) 1367–1383.
- [3] Y. Liu, D. Tipper, K. Vajanapoom, Spare capacity allocation in two-layer networks, *IEEE Journal on Selected Areas in Communications* 25 (5) (2007) 974–986.
- [4] R. Doverspike, B. Cortez, Restoration in carrier networks, in: *Proceedings of the IEEE DRCN*, October 2009.
- [5] M. Jaeger, R. Huelsermann, Service availability of shared path protection in optical mesh networks, in: *Proceedings of the European Conference on Optical Communication (ECOC)*, September 2004, We4.P.154.
- [6] J. Zhang, K. Zhu, H. Zang, N.S. Matloff, B. Mukherjee, Availability-aware provisioning strategies for differentiated protection services in wavelength-convertible WDM mesh networks, *IEEE/ACM Transactions on Networking* 15 (5) (2007) 1177–1190.
- [7] L. Song, J. Zhang, B. Mukherjee, Dynamic provisioning with availability guarantee for differentiated services in survivable WDM mesh networks, *IEEE Journal on Selected Areas in Communications, Supplement on Optical Communications and Networking* 25 (4) (2007) 35–43.
- [8] D.A.A. Mello, D.A. Schupke, H. Waldman, A matrix-based analytical approach to connection unavailability estimation in shared backup path protection, *IEEE Communications Letters* 9 (9) (2005) 844–846.
- [9] L. Zhou, M. Held, U. Sennhauser, Connection availability analysis of shared backup path-protected mesh networks, *IEEE/OSA Journal of Lightwave Technology* 25 (5) (2007) 1111–1119.
- [10] D.A.A. Mello, H. Waldman, Analytical bounds on the unavailability of protected connections in WDM optical networks, *IEEE Communications Letters* 11 (11) (2007) 901–903.
- [11] A. Markopoulou, G. Iannaccone, S. Bhattacharyya, C.-N. Chuah, Y. Ganjali, C. Diot, Characterization of failures in an operational IP backbone network, *IEEE/ACM Transactions on Networking* 16 (4) (2008) 749–762.
- [12] W. Yao, B. Ramamurthy, Survivable traffic grooming with differentiated end-to-end availability guarantees in WDM mesh networks, in: *Proceedings of the IEEE LANMAN*, April 2004.
- [13] M. Tornatore, et al., Grooming and protection with availability guarantees in multilayer optical networks, in: *Proceedings of the IEEE ONDM*, February 2009.
- [14] M. Tornatore, D. Lucerna, B. Mukherjee, A. Pattavina, Multilayer protection with availability guarantees in optical WDM networks, *Springer Journal of Network and Systems Management* 20 (1) (2012) 34–55.
- [15] H.-W. Lee, E. Modiano, K. Lee, Diverse routing in networks with probabilistic failures, *IEEE/ACM Transactions on Networking* 18 (6) (2010) 1895–1907.
- [16] K. Lee, H.-W. Lee, E. Modiano, Reliability in layered networks with random link failures, *IEEE/ACM Transactions on Networking* 19 (6) (2011) 1835–1848.
- [17] A.L. Chiu, et al., Network design and architectures for highly dynamic next-generation IP-over-optical long distance networks, *IEEE/OSA Journal of Lightwave Technology* 27 (12) (2009) 1878–1890.
- [18] W. Ni, J. Wu, C. Huang, M. Savoie, Flow availability analysis in two-layer networks with dedicated path protection at the upper layer, in: *Proceedings of the IEEE ICC*, June 2012.
- [19] E. Modiano, A. Narula-Tam, Survivable lightpath routing: a new approach to the design of WDM-based networks, *IEEE Journal on Selected Areas in Communications* 20 (4) (2002) 800–809.
- [20] K. Lee, E. Modiano, H.-W. Lee, Cross-layer survivability in WDM-based networks, *IEEE/ACM Transactions on Networking* 19 (4) (2011) 1000–1013.
- [21] P. Pacharintanakul, D. Tipper, The effects of multi-layer traffic on the survivability of IP-over-WDM networks, in: *Proceedings of the IEEE ICC*, June 2009.
- [22] K.S. Ho, V.Y. Liu, Traffic grooming in WDM mesh networks with loop-free paths, in: *Proceedings of the IEEE/OSA OFC/NFOEC*, March 2012.
- [23] A.L. Chiu, et al., Architectures and protocols for capacity efficient, highly dynamic and highly resilient core networks, *IEEE/OSA Journal of the Optical Communications and Networking* 4 (1) (2012) 1–14.
- [24] M. To, P. Neusy, Unavailability analysis of long-haul networks, *IEEE Journal on Selected Areas in Communications* 12 (1) (1994) 100–109.
- [25] W. Ni, Y. Ye, M. Schlosser, E. Patzak, H. Zhang, Survivable mapping with maximal physical-layer failure-localization potential in IP over transparent optical networks, in: *Proceedings of the IEEE/OSA OFC*, March 2010.
- [26] R. Bhandari, *Survivable Networks Algorithms for Diverse Routing*, Kluwer Academic Publishers, Boston, MA, 1999.
- [27] D.A.A. Mello, H. Waldman, G.S. Quitério, Interval availability estimation for protected connections in optical networks, *Elsevier Computer Networks* 55 (1) (2011) 193–204.
- [28] S.M. Ross, *Introduction to Probability Models*, Elsevier Academic Press, 2003.